PERGAMON

Deep-Sea Research I 48 (2001) 1255–1277

DEEP-SEA RESEARCH
PART I

www.elsevier.com/locate/dsr

Comparing the overflow of dense water in isopycnic and cartesian models with tracer observations in the eastern Mediterranean

Vassil M. Roussenov[a,*], Richard G. Williams[a], Wolfgang Roether[b]

[a]*Oceanography Laboratories, Department of Earth Sciences, University of Liverpool, P.O. Box 147, Liverpool L69 3BX, UK*
[b]*Institut für Umveltphysik, University of Bremen, Bremen, Germany*

Received 2 August 1999; received in revised form 19 January 2000; accepted 3 July 2000

Abstract

Isopycnic and cartesian model simulations for the overflow and spreading of dense water are compared with each other and with independent transient-tracer observations. This case study is performed for Adriatic dense water overflowing into the deep eastern Mediterranean with chlorofluoromethane (CFC-12) observations used to test the model simulations. The realism of both types of model simulation depends on the representation of diapycnal mixing. In the cartesian model, convective adjustment and mixing dilute the overflow of Adriatic dense water and lead to unrealistic vertical homogenization. Incorporating a modified convection scheme emphasizing the sinking of dense fluid, rather than its mixing, leads to a more realistic penetration of the dense overflow. In the isopycnic model, there is an improved simulation of the overflow, which leads to the density contrast of the deep Mediterranean waters being maintained. However, there is too low a CFC-12 concentration at mid-depths unless explicit diapycnal mixing is incorporated. In each model, the different spreading of dense water is associated with a different bottom pressure torque and depth-integrated transport, and hence with contrasting tracer distributions throughout the water column.

Keywords: Overflow; Deep Water formation; Slope processes; Tracer modelling; Eastern Mediterranean Sea

1. Introduction

Most dense waters spread away from their formation sites into the deep ocean through overflows, descending down topography, into the ocean interior. Mixing and dilution of water

* Corresponding author.
E-mail address: vassilr@liv.ac.uk (V.M. Roussenov).

0967-0637/01/$ - see front matter
PII: S0967-0637(00)00082-0

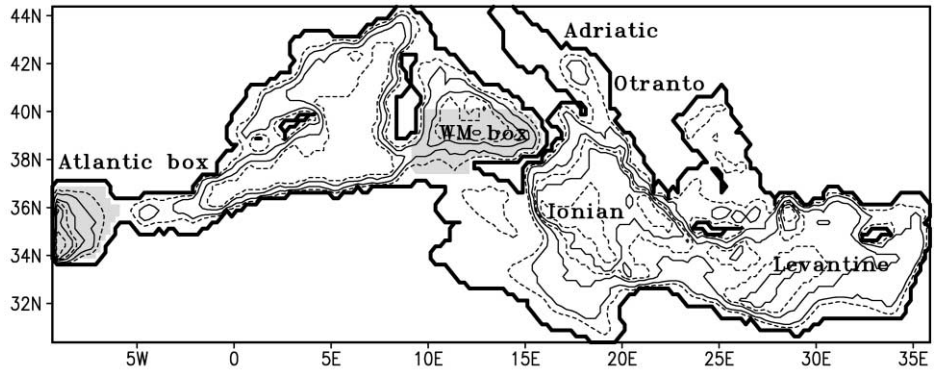

Fig. 1. Model domain and topography over the Mediterranean (full contours every 1000 m and dashed contours at 500, 2500 and 3500 m). The spreading of dense water is examined from the Adriatic into the Ionian via the Otranto Strait at 39°N. Shaded regions correspond to internal restoring boxes in the Atlantic for MOMA and in the western Mediterranean for MICOM.

masses at these overflows determines the level at which the dense water spreads over the ocean interior (Price and Baringer, 1994). Circulation models usually misrepresent this overflow process and either have too much associated mixing in cartesian models (Beckmann and Döscher, 1997) or too little in isopycnic models. These differences have far reaching consequences leading to different water-mass structures and circulations, as revealed in model comparisons for the North Atlantic (Roberts et al., 1996; DYNAMO, 1997). Winton et al. (1998) show that a similar downslope flow is obtained from isopycnic and cartesian models in an idealized study provided that the cartesian model resolves the bottom Ekman layer and the maximum slope of the topography.

In this study, we examine the spreading of dense water in cartesian and isopycnic models for a realistic setting and compare with independent transient-tracer observations. A case study is performed for the spreading of Adriatic dense water over the eastern Mediterranean. Adriatic dense water plays an important role in the thermohaline circulation of the eastern Mediterranean (Fig. 1): dense water is formed every winter in the Adriatic, spreads into the Ionian, and usually forms the main source of eastern Mediterranean dense water. The ventilation process is clearly revealed by observations of the transient tracer chlorofluoromethane (CFC-12) in 1987 (Roether and Schlitzer, 1991; Schlitzer et al., 1991), which have been modelled by Roether et al. (1994) and Beitzel (1997). In these cartesian modelling studies, one of the main difficulties was too much mixing occurring at density overflows (also see Wu and Haines, 1996). We now extend these cartesian modelling studies by employing an isopycnic model, in which dense overflows are more naturally represented in terms of a propagation of dense layers over the topography. The cartesian and isopycnic models are integrated for the same domain with similar forcing functions and resolution, and include on-line simulations of CFC-12 in order to allow precise comparison with the observations.

2. Observations of the thermohaline circulation in the eastern Mediterranean

The thermohaline circulation of the eastern Mediterranean is characterized by external and internal cells. The external cell consists of an inflow of fresh, warm waters of Atlantic origin through

the Strait of Sicily, which are converted into denser waters by evaporation and subsequent cooling in winter. The dense return flow through the Strait of Sicily is dominated by the Levantine Intermediate Water (henceforth LIW) (Wüst, 1961), which is formed primarily around the Rhodes gyre in the northwest Levantine.

The internal cell consists of denser water formed in the Aegean and Adriatic, which spreads below the LIW, but essentially remains confined within the eastern Mediterranean. The lower intermediate waters usually originate from the South Aegean (Schlitzer et al., 1991) and the deep waters below 1200 m from the Adriatic (Ovchinnkov et al., 1985). This internal cell has recently changed with the most dense water being formed in the South Aegean leading to an uplift of the old bottom waters across the eastern Mediterranean (Roether et al., 1996). In this study, we choose to focus on the state of the deep waters before this transient event.

The formation and spreading of Adriatic Deep Water consists of several stages: (i) preconditioning involving a salinity increase within the Adriatic due to inflow of LIW, (ii) dense water formation in the Southern Adriatic after intense winter cooling, followed by deep convection reaching the bottom, (iii) dense water overflow across the Otranto Strait sill spreading at a typical rate of 0.3 Sv (1 Sv $= 10^6$ m^3 s^{-1}) along a western boundary current into the deep Ionian (Roether and Schlitzer, 1991), and (iv) eventually, spreading of the dense waters eastward partly overflowing the sills between the Ionian and Levantine. This thermohaline circulation is closed predominantly by diapycnal transfer within the eastern Mediterranean.

In our study, we focus on the spreading of Adriatic Deep Water and compare with hydrographic and tracer data from Meteor cruise no. 5, leg 6, 1987 (hereafter Meteor 87), which has been reported in detail by Roether and Schlitzer (1991) and Schlitzer et al. (1991). A north–south section through the Ionian reveals the bottom waters (defined by $\sigma_0 > 29.185$) connected to the northern source in the Adriatic (Fig. 2a). Away from the northern slope, the deep waters below 1500 m are very homogeneous in density and only contain small contrasts of typically 0.003 in the interior. There are high CFC-12 concentrations (greater than 0.2 pmol kg^{-1}) in the bottom waters connected to the northern source (Fig. 2b). Elsewhere, there are low CFC-12 concentrations at mid-depths, which reveals that this region is not strongly ventilated from the Adriatic. This low concentration extends over the mid-depths of the entire Levantine basin (Schlitzer et al., 1991), which reflects the lack of recent ventilation before the observations in 1987.

The dynamic tracer, large-scale potential vorticity[1] (PV) generally decreases with depth from at least 1×10^{-12} m^{-1} s^{-1} in the thermocline to less than 0.1×10^{-12} m^{-1} s^{-1} at 2500 m and below (Fig. 2c). There is a signature of slightly higher PV in the bottom waters of 0.2×10^{-12} m^{-1} s^{-1} in the northern Ionian. The CFC-12 signal suggests that this higher PV on the bottom is recently ventilated. The minimum in PV at 2500 m south of 36°N might be a relic of previous ventilation events which happened to produce lower PV or alternatively result from enhanced mid-depth mixing.

We now examine how two different circulation models simulate these transient and dynamic tracer distributions over the eastern Mediterranean.

[1] The large-scale potential vorticity is evaluated from $-(f/\bar{\rho})\partial\sigma_3/\partial z$ where f is the Coriolis parameter, σ_3 is the potential density referenced to a depth of 3 km and $\bar{\rho}$ is the reference density.

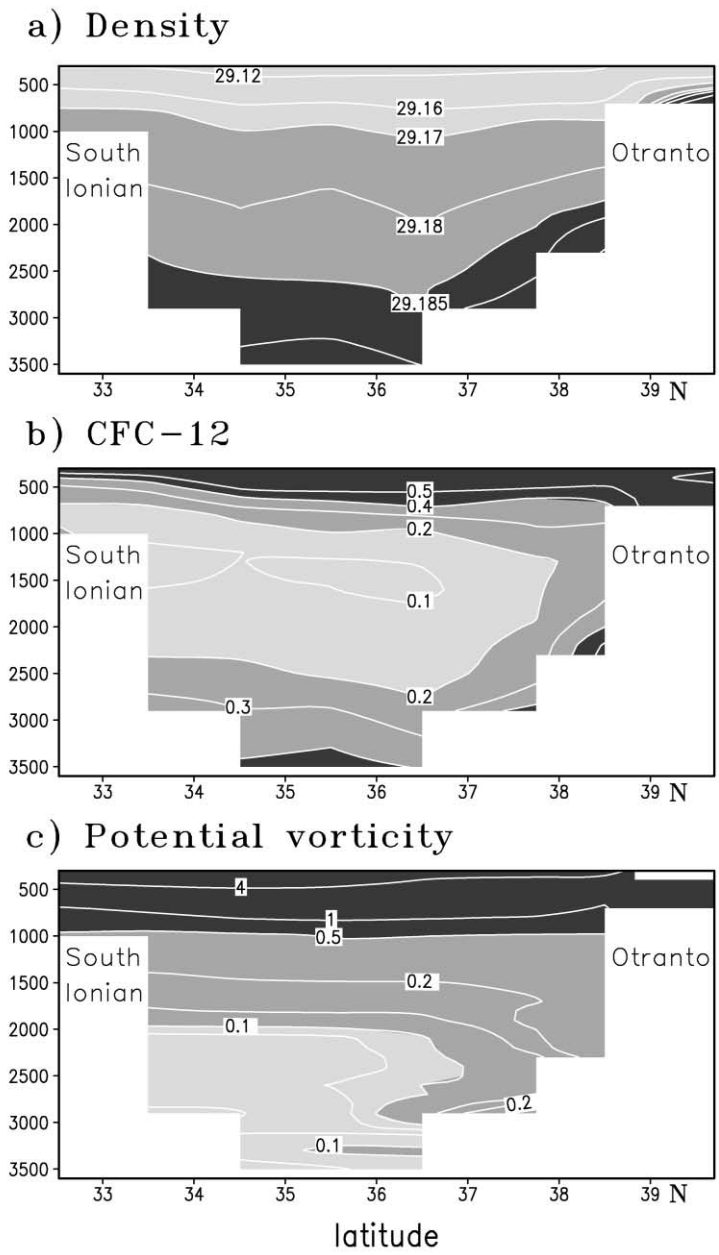

Fig. 2. Meteor'87 north–south section through the Ionian along 18.6°E : (a) potential density σ_0, (b) CFC-12 (pmol kg^{-1}) and (c) large-scale potential vorticity (10^{-12} m^{-1} s^{-1}). Note that the upper 300 m is suppressed in the plots.

3. Model descriptions

Previous modelling studies of the Mediterranean have simulated the upper and intermediate circulation, but have had difficulties in correctly representing the formation and spreading of dense

water. In particular, there have been problems in the representation of the overflow and slope convection process. Consequently, we focus on modelling this aspect of the thermohaline circulation.

3.1. Cartesian model

We employ a free sea surface, cartesian model (referred to as MOMA; Webb et al., 1997) over the Mediterranean. The model resolution is 1/4° in the horizontal and 31 levels in the vertical with a vertical spacing increasing from 10 m below the sea surface to 300 m below 1000 m depth. The model incorporates a flux-limiter advection scheme for tracers (Stratford, 1999), which is positively definite with negligible numerical diffusivity, and an adiabatic, sub-gridscale parameterization (Gent and McWilliams, 1990; henceforth GM). Incorporating the flux-limiter advection scheme and adiabatic sub-gridscale parameterization reduces substantially cross-isopycnic mixing, which is usually a characteristic defect of cartesian models.

The model integrations are conducted without any explicit horizontal and vertical diffusion in the temperature, salt and tracer equations, apart from a small value of 50 $m^2\ s^{-1}$ for the thickness diffusion for the GM parameterization. Turbulent mixing is incorporated in the momentum equation in a biharmonic form in the horizontal with a coefficient of $3\times10^{10}\ m^4\ s^{-1}$ and a Laplacian in the vertical with coefficients decreasing from $1.5\times10^{-4}\ m^2\ s^{-1}$ at the surface to a uniform value of $1.5\times10^{-6}\ m^2\ s^{-1}$ at 180 m and below. The free-surface model uses barotropic–baroclinic time-splitting procedure with time steps of 60 and 3600 s, respectively.

3.2. Isopycnic model

We employ a coupled mixed-layer and isopycnic model (referred to as MICOM version 2.7; Bleck and Smith, 1990), which is integrated over the eastern Mediterranean. The resolution is 25 km in the horizontal and 14 layers in the vertical with densities ranging from 27.60 to 29.22 sigma units. While the number of layers in the isopycnic model is fewer than the number of levels in the cartesian model, there is a similar resolution below 1000 m where MOMA has 10 levels spaced 300 m apart and MICOM has 9 isopycnic layers.

MICOM also employs a free surface, a similar time-splitting procedure and an advanced advection scheme, although formulated in terms of a flux-correction scheme, rather than a flux-limiter scheme. The momentum mixing is deformation dependent with a background Laplacian mixing and a turbulent mixing velocity of 1 cm s^{-1}. Isopycnic mixing is included with a standard Laplacian form and a diffusive velocity of 0.2 cm s^{-1}. The diapycnic diffusion is chosen either to have a constant value (10^{-5} or $10^{-4}\ m^2\ s^{-1}$) or to vary inversely with buoyancy frequency (varying between the above constant values).

The model includes a vertically homogeneous mixed layer represented by a single non-isopycnic layer which allows horizontal density variations. The mixed-layer thickness is predicted from the surface forcing using a turbulent kinetic energy balance. Fluid within the mixed layer may be exchanged with any of the other model layers as long as the density matches. Individual layers can inflate or collapse to a vanishing thickness.

3.3. Boundary conditions and forcing

Both models use the same surface boundary conditions for the wind stress, sea-surface temperature (SST), sea-surface salinity (SSS) and bottom topography. They are those employed by Roussenov et al. (1995), except that topography has increased vertical resolution. Bottom topography (Fig. 1) resolved in MOMA depends on the horizontal and vertical grid spacing. Fine-scale topographic features are lost in the deep basin where the vertical spacing is only 300 m. In addition, the deep tracer field can become isolated from advection in narrow channels through the different positions of the tracer and velocity points on the B-grid for MOMA. The same restrictions do not apply in MICOM and the representation of the bottom topography only depends on the horizontal resolution. However, we choose to use the same degraded topography in MICOM as in MOMA in order to aid the comparison of the model results.

The models are initialized using annual-mean temperature and salinity distributions from Levitus (1982), and initial isopycnic depths are calculated using the same equation of state as in MICOM (Friedrich and Levitus, 1972).

In order to maintain the correct surface properties, we employ an unphysical relaxation of the SST and SSS to climatological values, rather than impose poorly known surface fluxes. Following Wu and Haines (1996), we adopt a restoring timescale of 2 h for SST everywhere and 5 days for SSS (apart from over the Rhodes gyre where the relaxation is reduced to 2 h in order to ensure LIW formation). Previous cartesian modelling studies have produced too light an Adriatic water mass when restoring to monthly mean SST and SSS. In our cartesian simulation, we only form Adriatic deep water with the correct density if we include restoring to SST cooler than the monthly mean by 0.6°C over a timescale of 6 days; note that this additional restoring is less severe than that applied by Roether et al. (1994).

Each model represents the open boundary to the west by incorporating an extra box to simulate the neighbouring basin (shaded regions in Fig. 1). Within this box, the temperature and salinity are restored throughout the water column to the climatology on a minimum timescale of 1 day. The western box is the Atlantic for the cartesian model and the western Mediterranean for the isopycnic model; this difference is relatively unimportant for the deep circulation below the sill. Applying this boundary condition leads to a reasonable exchange through the Gibraltar and Sicily Straits.

Both models are integrated in 'perpetual year' mode with seasonally varying, surface boundary conditions for an initial spin-up of 12 years and then including a CFC-12 simulation for a further 28 years.

3.4. Modelled density structure

The annual-mean Levitus climatology, used to initialize the model integrations, does not show a signal of the bottom water in the Ionian originating from the Adriatic (Fig. 3a), as implied in the previous Meteor'87 observations for the same section (Fig. 2a). However, after 40 years of integration, both models produce dense Adriatic water, which spreads over the slope and throughout the deepest part of Ionian and fills its central part with newly formed deep waters (Fig. 3b and c); the solutions shown here are for the optimal cases discussed later in Section 5. The source of the deep water can be traced through doming of dense isopycnals to the Otranto Strait at 39°N. While the modelled density structure appears similar to that observed, there is a higher value of the deep

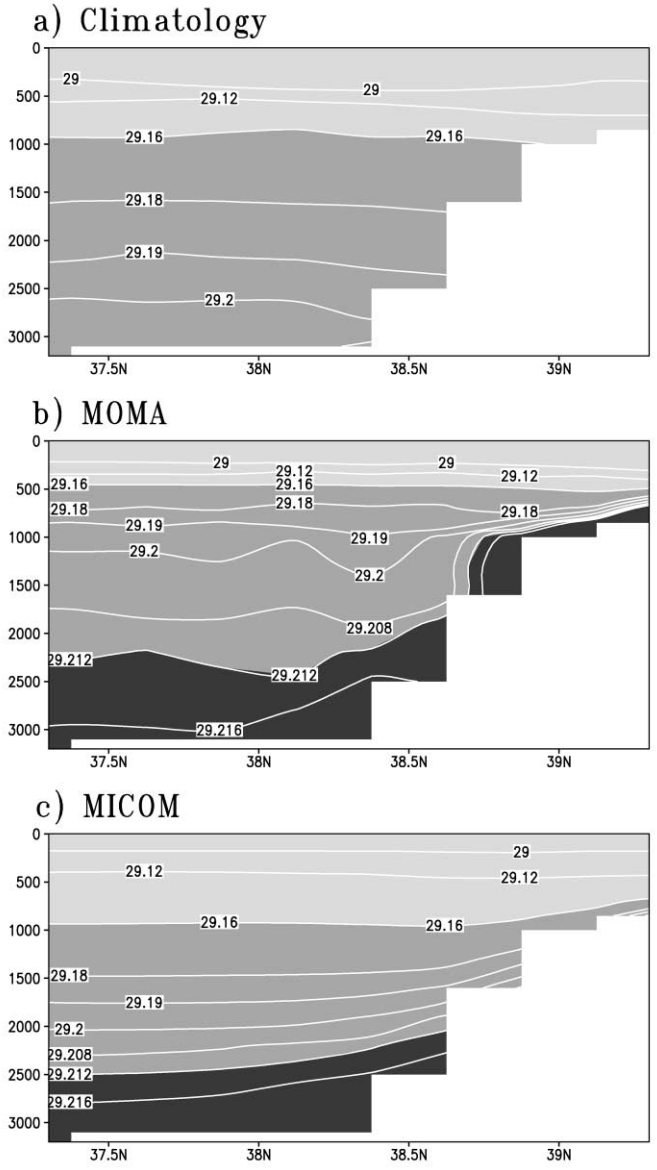

Fig. 3. North–south sections of σ_0 through the northern Ionian along 18.6°E (with the Otranto Strait at 39°N): (a) initial field from Levitus climatology, and modelled at year 40 using optimal integrations of (b) MOMA and (c) MICOM.

density in the model, which arises from initializing with climatology, rather than from Meteor'87 data.

There are marked oscillations in the height of isopycnals close to the topography in MOMA (Fig. 3b) consistent with enhanced mixing occurring, whereas the oscillations are absent in MICOM (Fig. 3c). The spreading and mixing of dense water is more clearly revealed by examining

the transient-tracer distributions: firstly, we conduct sensitivity experiments in Section 4 and, secondly, we compare the optimal model solutions with the observations.

4. Sensitivity experiments for the transient tracer

The CFC-12 concentrations are modelled on-line using sea-surface boundary conditions evaluated from the time history of the atmospheric CFC-12 dry-air mixing ratio, which is converted into surface water concentrations, assuming a solubility equilibrium, using a solubility function depending on SST and SSS (Warner and Weiss, 1985). The assumption of near equilibrium is generally supported by a previous modelling study of Roether et al. (1994), although CFC deficits relative to a solubility equilibrium have been observed locally during deep convection (Klein et al., 1999) and in overflow waters in the Strait of Otranto (Schlitzer et al., 1991). In practice, our model results appear to reasonably capture the observed seasonal cycle in CFC-12: in summer, the higher SST and lower solubility leads to surface concentrations of 0.9–1 pmol kg^{-1} with a subsurface maximum of about 1.2 pmol kg^{-1} at 50–100 m depths (see Fig. 17 in Roether et al., 1994).

The tracer results are sensitive to the levels of mixing in both the cartesian and isopycnic integrations. Therefore, in both types of model, we conduct sensitivity experiments examining the transient-tracer distribution and their dependence on diapycnal mixing.

4.1. MOMA simulation and the convection scheme

For MOMA, we conduct two experiments with either artificially high or realistic outflows of dense water through Otranto Strait, which are obtained by altering the temperature that the SST is relaxed to in winter over the Adriatic. In either case, there is a relatively poor simulation for CFC-12 when using a traditional convection scheme. There is either too much vertical homogenization when dense water is formed and overflows the sill (Fig. 4a) or the overflow water is diluted so much that none reaches the sea floor (Fig. 4b), which is contrary to the observations (Fig. 2b). The overly high mixing is partly a result of the traditional convection scheme, which leads to vertical homogenization whenever dense fluid overlies light fluid.

In this study, we adopt a different convective scheme emphasizing the sinking of dense water, rather than its mixing. Any dense fluid overlying lighter fluid is vertically transferred to its neutrally buoyant level and lighter fluid is displaced upwards; see more details of the scheme in the appendix (Fig. 13) and a previous application in Roether et al. (1994). A similar approach involving the direct transfer of dense waters in a bottom boundary layer scheme has been developed by Beckmann and Döscher (1997). Applying this alternative convection scheme leads to dense Adriatic waters reaching the deepest Ionian, as well as the water-mass flux through the dense water outflow of the Otranto Strait being comparable to observations by Roether and Schlitzer (1991). There is an improved CFC-12 distribution (Fig. 4c), which is much closer to that observed (Fig. 2b). While other model studies have also formed these dense waters, they have obtained them at the cost of the water-mass fluxes through Otranto Strait being unrealistically high. This model solution with the convective exchange scheme is the optimal MOMA case discussed further in Section 5.

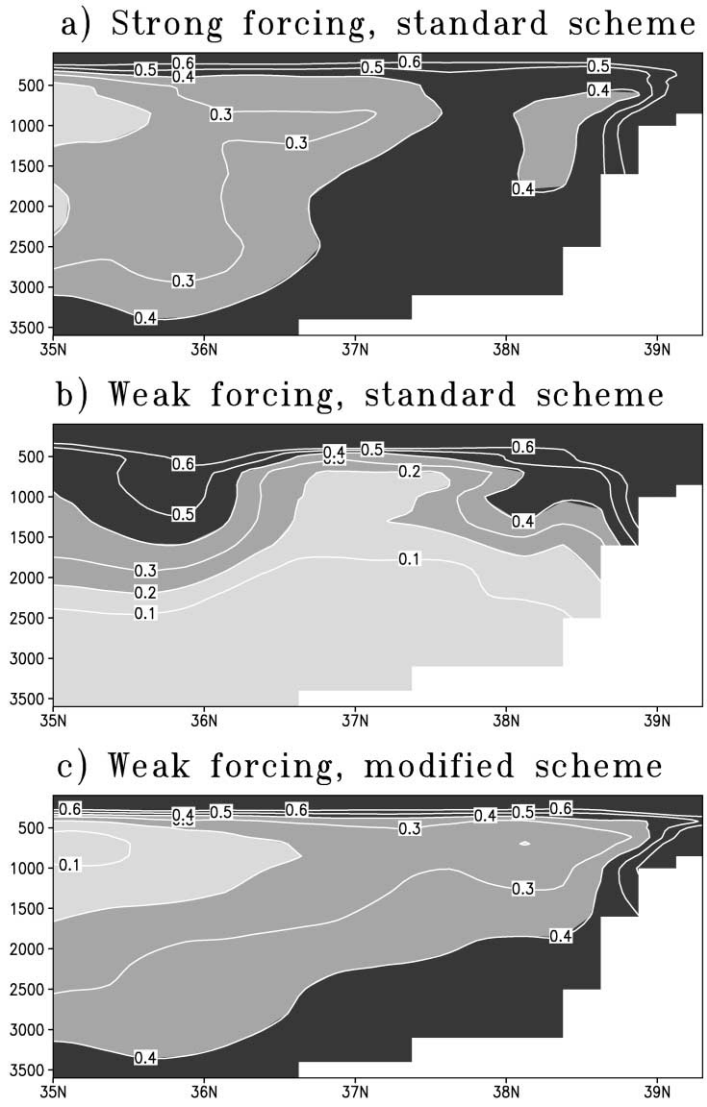

Fig. 4. Sensitivity experiments for MOMA at year 40 showing a north–south section of CFC-12 (pmol kg^{-1}) through the northern Ionian along 18.6°E: firstly, using the traditional, vertical homogenization, convection scheme for overflows that are strongly and weakly forced in (a) and (b); secondly, using a vertical exchange, convection scheme in (c) with the same surface forcing as applied in (b), which is referred to as the optimal MOMA case.

4.2. MICOM simulation and the diapycnic mixing

For MICOM, the extent of dense water spreading is controlled by both the volume flux from the source in the Adriatic and the explicit diapycnal transfer to lighter surfaces. It is unclear what value the diapycnic diffusivity should locally be. Basin-scale values of $\kappa \sim 1 \times 10^{-4}$ m^2 s^{-1} have been

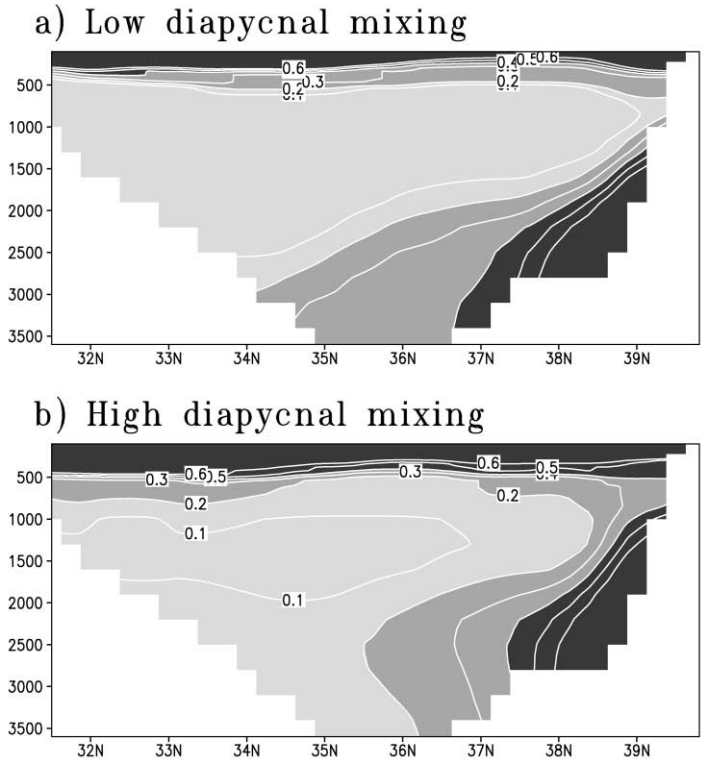

Fig. 5. Sensitivity experiments for MICOM at year 40 showing a north–south section of CFC-12 (pmol kg^{-1}) through the northern Ionian along 18.3°E: (a) low diapycnal diffusivity, $\kappa = 10^{-5}$ m^2 s^{-1}; (b) high diapycnal diffusivity, $\kappa = 10^{-4} m^2$ s^{-1}.

estimated from tracer observations (Roether et al., 1994), although local in situ measurements of κ are often an order of magnitude smaller.[2]

Accordingly, two experiments are conducted with a constant diapycnal diffusivity of a low or high magnitude of 10^{-5} or 10^{-4} m^2 s^{-1}, respectively. The modelled tracer invades the deep basin more and the mid-depths less in the low-diffusivity case, compared with the high-diffusivity case (Fig. 5). The observed tracer distribution shown in Fig. 2b appears to be between these two modelled cases. The increased diapycnal mixing in MICOM prevents the penetration of dense waters into the deepest region and produces CFC-12 distribution in the North Ionian closer to MOMA simulation.

[2] There have not been in situ measurements of κ in the eastern Mediterranean. Elsewhere, in situ measurements of κ have low values of 10^{-5} m^2 s^{-1} for the mid-thermocline (Ledwell et al., 1993) and higher values confined to the ocean bottom (Toole et al., 1997) and above rough topography (Polzin et al., 1997). This enhanced mixing has been associated with internal wave generation from barotropic tides interacting with rough topography (Munk and Wunsch, 1998). Consequently, a lower value for κ of the order of 10^{-5} m^2 s^{-1} might be appropriate for the eastern Mediterranean, since the tides are relatively weak in this nearly confined basin. Alternatively, there can still be wind-induced, self-oscillations, which might generate internal waves and associated mixing.

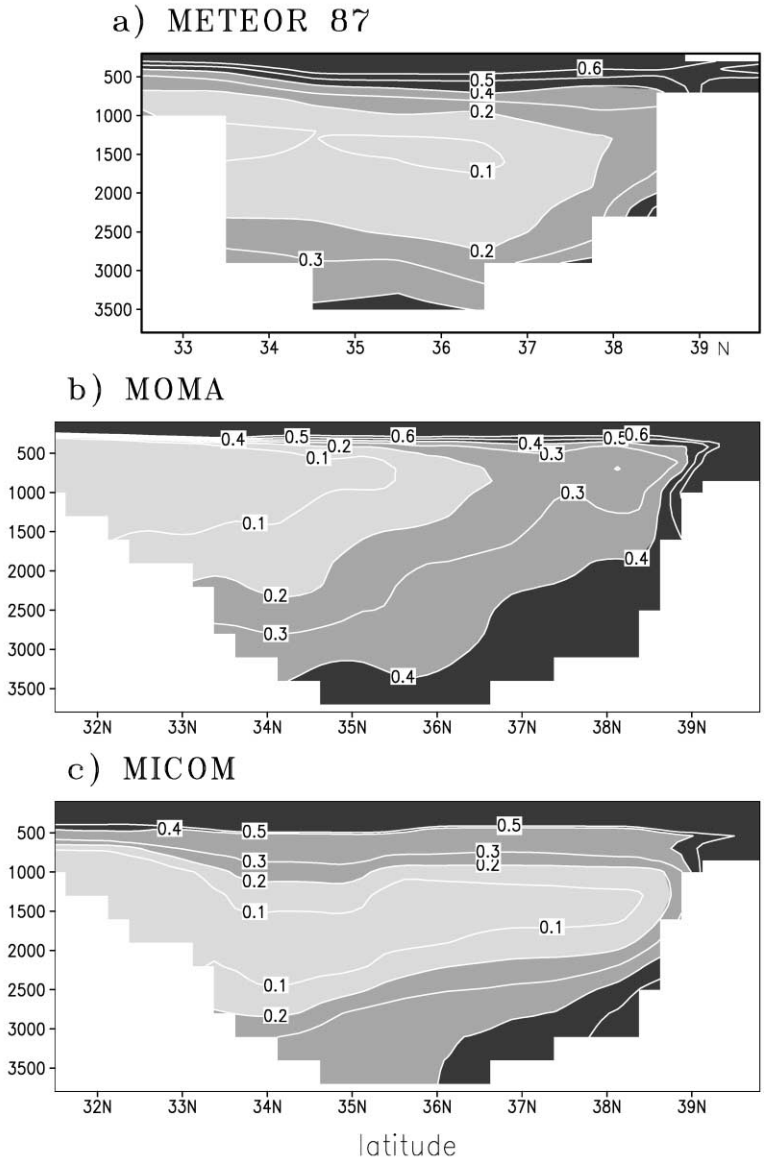

Fig. 6. North–south sections of CFC-12 (pmol kg^{-1}) through the Ionian along 18.6°E: (a) Meteor'87 observations, and modelled at year 40 using optimal integrations of (b) MOMA and (c) MICOM.

Therefore, our optimal integration with MICOM uses a spatially variable diffusivity where $\kappa = 10^{-8}/N$ and N is the buoyancy frequency. Incorporating this parameterization of enhanced mixing where there is low stratification leads to κ varying from 3×10^{-5} m^2 s^{-1} in the deep basin, between 1 and 2×10^{-5} m^2 s^{-1} in the interior of the basin below 1 km, and reducing to 0.5×10^{-5} m^2 s^{-1} in the overflow where there is strong stratification. The tracer results for this case (Fig. 6c) are compared with the observations and the optimal results from the cartesian model in Section 5.

5. Comparison of model simulations and tracer observations

The optimal MOMA and MICOM simulations are now used to investigate the CFC-12 distributions in more detail, including an analysis of the tracer fields, a volumetric budget, the potential vorticity distribution, and the connection between the bottom pressure torque and barotropic circulation.

5.1. CFC-12 distribution

The CFC-12 distribution from Meteor'87, and the optimal model solutions from MOMA and MICOM are shown together in Fig. 6. There is a broadly similar structure in the observations and the model results with high CFC-12 in the upper thermocline and the bottom waters (>0.4 pmol kg^{-1}), which is separated by a mid-depth minimum (<0.2 pmol kg^{-1}) between 500 and 2000 m marking the oldest waters. The bottom waters are ventilated by the overflow of Adriatic dense water through the Otranto Strait (at 39°N). However, the different representation of mixing in each model still leads to differences in the CFC-12 distribution.

The CFC-12 distribution from MOMA is broadly similar to that observed over the southern Ionian, but is more different over the northern Ionian (Figs. 6a and b). The modelled mid-depth minimum only extends to 36.5°N, rather than as observed to almost 38°N. The higher mid-depth CFC-12 concentration is a result of slope convection occurring through the dense water sinking along the stepwise topography, leading to enhanced cross-isopycnal mixing. While in reality there should be additional mixing over rough topography (Price and Baringer, 1994), the tracer simulations suggest that the cartesian model exaggerates the mixing.

The CFC-12 distribution from MICOM is much closer to that observed over the whole Ionian (see Fig. 6c), than obtained with MOMA. The high concentration in the bottom waters is acquired through dense fluid overflowing through the Otranto Strait, propagating down the topography and preserving much of their tracer contrast. The mid-depth minimum extends over most of the Ionian. There is no signal of implicit cross-isopycnal mixing over the topography and no vertical homogenization over the northern Ionian.

A west–east section of the CFC-12 distribution reveals differences in the mid-depth waters. The unventilated waters at mid-depths are observed to extend east of 17°E (Fig. 7a), but only extend east of 18°E in MOMA (Fig. 7b) and instead extend over most of the section for MICOM (Fig. 7c). Maps of the transient tracer along the bottom reveal high CFC-12 spreading southwestwards along the western boundary (Fig. 8). The CFC-12 concentrations are higher to the west in MICOM which is also in better agreement with the observations (see Fig. 5b in Schlitzer et al., 1991), than in MOMA where stronger mixing dilutes the western source and increases the mid-basin concentrations.

The volume-weighted CFC-12 concentration over the Ionian is shown in Table 1 for Meteor'87 and the optimal MOMA and MICOM solutions. Below 1400 m, the observed CFC-12 concentrations are closer to the results of MICOM, than those of MOMA. This similarity holds if the analysis is repeated for sub-domains over the Ionian.

5.2. Volumetric analysis

The model results are now analysed in more detail in terms of a volumetric balance. The Meteor'87 observations reveal 0.3 ± 0.1 Sv of dense water overflowing through the Otranto Strait.

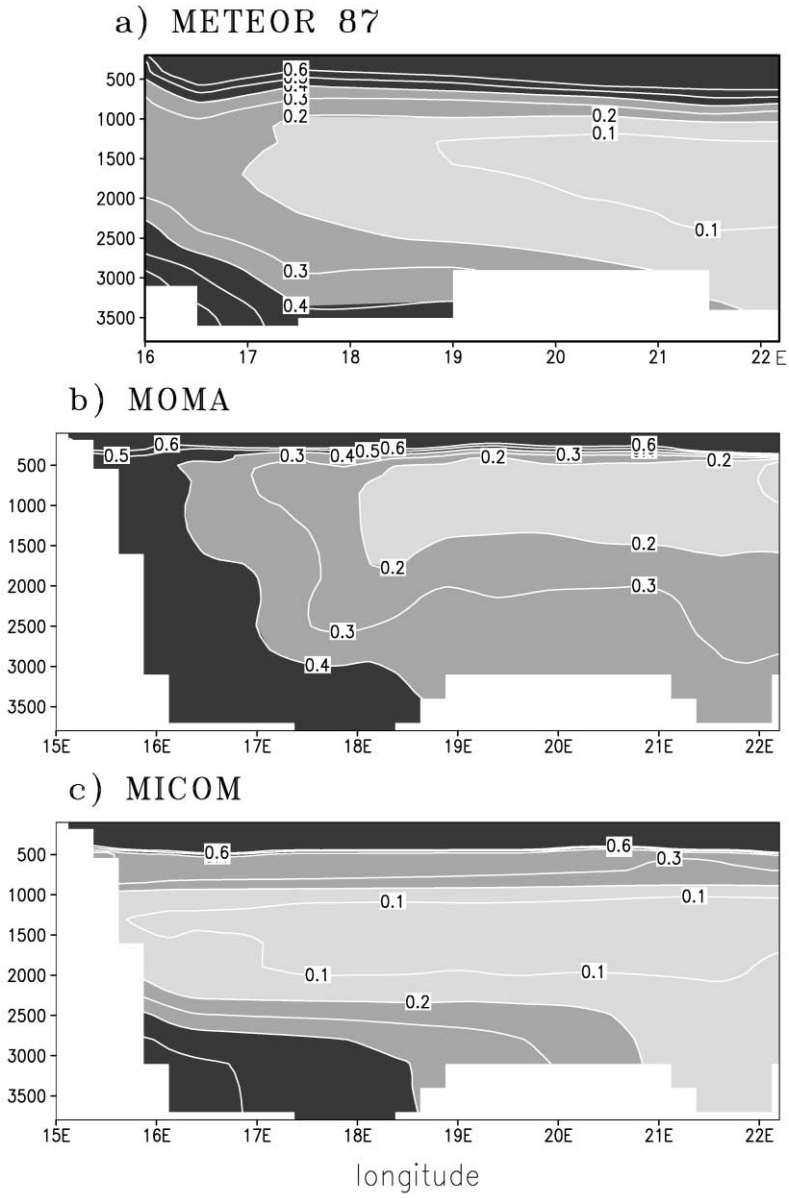

Fig. 7. West–east sections of CFC-12 (pmol kg^{-1}) through the Ionian along 35.5°N: (a) Meteor'87 observations, and modelled at year 40 using optimal integrations of (b) MOMA and (c) MICOM.

Most of this flux passes into the deep water below 1500 m in the Ionian (Roether and Schlitzer, 1991; Schlitzer et al., 1991).

In the MOMA simulation, dense water overflows at Otranto at a rate of 0.49 Sv and spreads through a sequence of convective sinking alongside topography, horizontal transport and vertical downwelling (Fig. 9a). This slope convection leads to an outflux of 0.8 Sv for the deep waters below

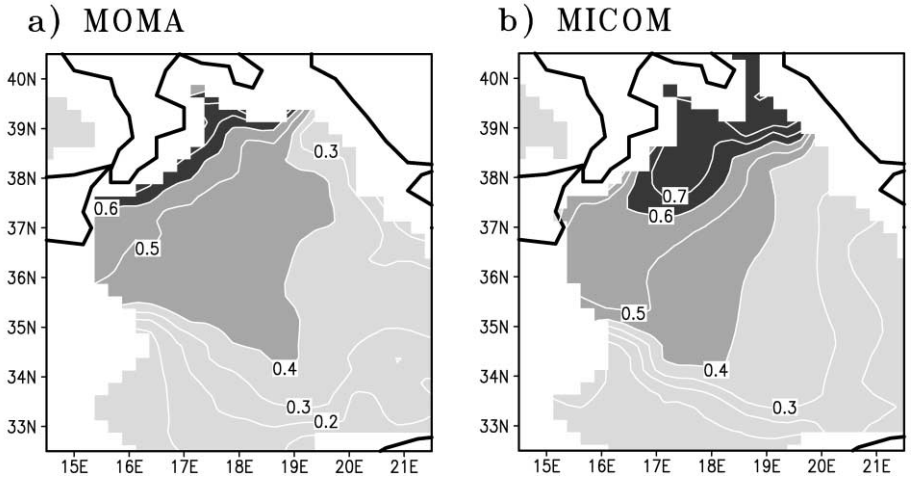

Fig. 8. Maps of CFC-12 (pmol kg^{-1}) at year 40 on the sea floor over the Ionian using optimal integrations of (a) MOMA and (b) MICOM.

Table 1
Volume-weighted CFC-12 concentration (pmol kg^{-1}) over the Ionian

Depth	Meteor'87	MOMA	MICOM
1000–1400 m	0.146	0.185	0.079
1400–1800 m	0.110	0.231	0.106
1800–2300 m	0.182	0.282	0.190
2300–bottom	0.320	0.361	0.342
1000–bottom	0.190	0.274	0.201

1300 m across 36.9°N, which is equally supplied by dense fluid originating from Otranto and fluid entrained from the mid-depths. There are large vertical fluxes, and cross-isopycnal fluxes, which reach 0.4 Sv.

The dense Adriatic water outflowing over the topography leads to hydrostatic instability. The convection scheme removes these instabilities by modifying temperature and salinity, such that dense water sinks to its neutrally buoyant level below the sill, usually to the bottom of the water column. The dense water spreads southwards along the Italian coast, consistent with the direction of a Kelvin wave propagation, and gradually sinks. The spreading of dense water leads to a horizontal divergence at the bottom level, which in turn leads to convergence and downwelling in the overlying column in order to satisfy continuity. This downwelling reaches a maximum in the regions involved in deep convection.

The volumetric balance for MICOM appears closer to the observations. The dense overflow through Otranto is 0.34 Sv and most of this flux, 0.29 Sv, spreads along dense layers ($\sigma_0 > 29.18$) below 1300 m at 36.9°N (Fig. 9b). At mid-depths, there are much weaker volume fluxes and the cross-isopycnal flux only reaches a maximum of 0.04 Sv.

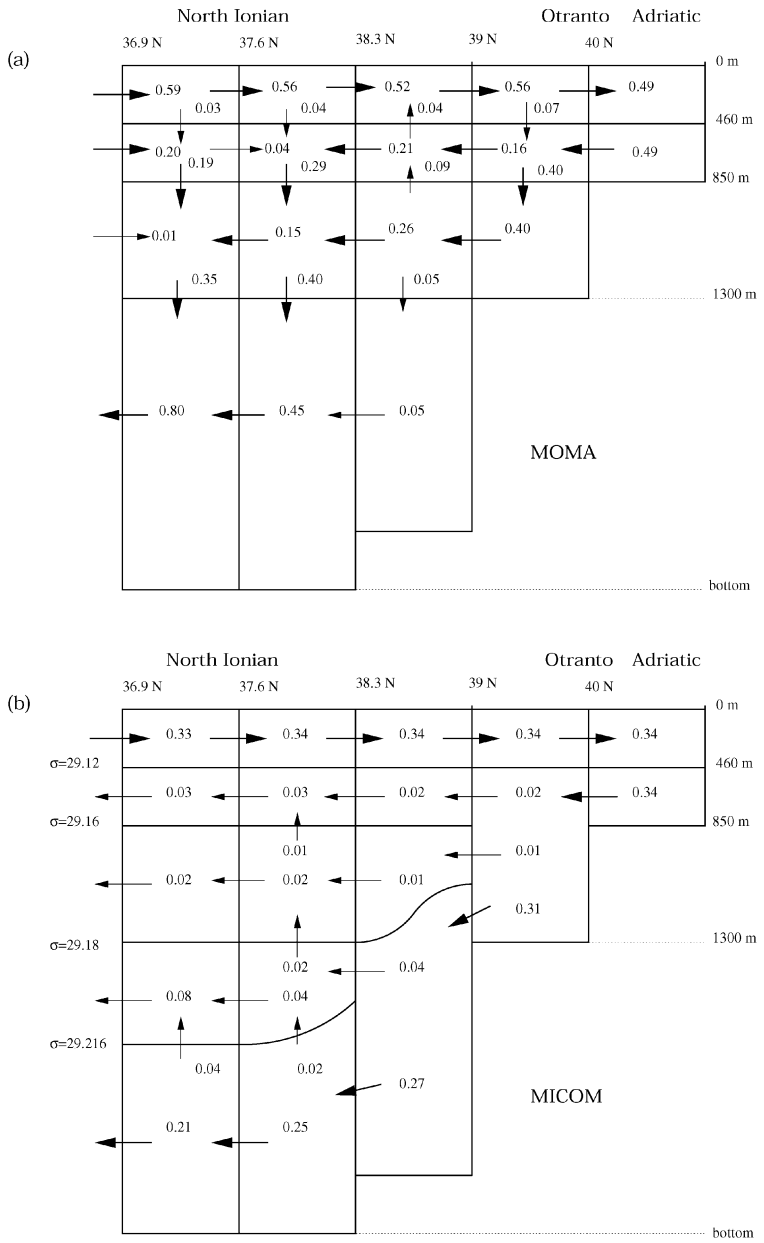

Fig. 9. Modelled zonal mean volume fluxes (Sv) for a north–south section through the Ionian at year 40 evaluated using optimal integrations of (a) MOMA along level surfaces and (b) MICOM along layers. Bold arrows refer to fluxes greater than 0.1 Sv.

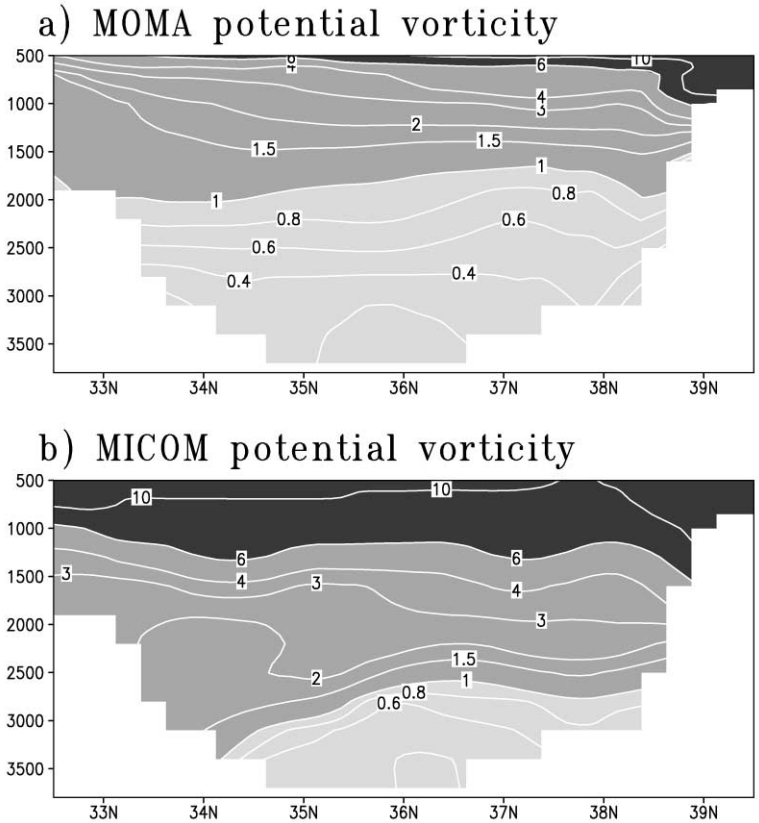

Fig. 10. Large-scale potential vorticity (10^{-12} m^{-1} s^{-1}) for a north–south section through the Ionian along 18.6°E at year 40 using optimal integrations of (a) MOMA and (b) MICOM. In comparison, the potential vorticity is shown for Meteor'87 in Fig. 2c.

5.3. Potential vorticity distribution

The modelled PV decreases with depth in both the MOMA and MICOM simulations (Fig. 10). The PV is generally lower in magnitude in MOMA with marked oscillations over the slope between 37°N and 39°N, compared with higher magnitudes and a smoother distribution in MICOM. These differences are consistent with there being greater cross-isopycnal mixing over the slope in MOMA. In both models, there is significant modification of the PV for the dense water overflowing the topography: the source water generally has high PV values near Otranto and the recently ventilated deep water (marked by high CFC-12) has lower PV values in the deep Ionian.

Neither model integration produces the mid-depth minimum in PV revealed in the observations (Fig. 2c). This mid-depth minimum might be a relic of the initial condition with previous ventilation forming lower PV, which is now older and without a CFC-12 signal. Alternatively, there might be enhanced mixing at mid-depth that reduces the PV, which is not adequately parameterized in either of the models.

5.4. Depth-integrated circulation and bottom pressure torque

There are contrasting horizontal circulations in MOMA and MICOM, as shown in Fig. 11, despite the same wind forcing and topography being applied. Over the northwestern Ionian, in MOMA, there is an intense cyclonic circulation extending to the sea floor with a barotropic velocity of typically 4 cm s^{-1} and a smaller baroclinic velocity of ± 2 cm s^{-1}. In contrast, in MICOM, there is an upper anticyclonic circulation and deeper cyclonic circulation with a smaller barotropic velocity of 1 cm s^{-1} and a larger baroclinic velocity of ± 3 cm s^{-1}.

The contrasting circulations in MOMA and MICOM may be understood through analysing the vorticity balance for the depth-integrated flow. Following Mertz and Wright (1992), depth integrating the linearized momentum equations and cross-differentiating gives

$$\frac{\partial}{\partial t} \nabla^2\psi + \beta\frac{\partial\psi}{\partial x} = \frac{1}{\rho_0} J(P_b, H) + \frac{1}{\rho_0} \mathrm{curl}_z(\tau_s - \tau_b), \tag{1}$$

where ψ is the streamfunction of the depth-integrated flow, β is the meridional gradient in the Coriolis parameter, P_b is the bottom pressure, H is the fluid depth, ρ_0 is the reference density, τ_s and τ_b are the surface and bottom stresses, and the Jacobian is defined by $J(A,B) \equiv (\partial A/\partial x)(\partial B/\partial y) - (\partial B/\partial x)(\partial A/\partial y)$. The time evolution of the vorticity of the depth-integrated flow balances the transport across planetary vorticity contours, the bottom pressure topographic torque, and the curl of the frictional stresses (see also Hughes, 2000). In our model integrations, in the northern Ionian, the dominant balance is between the transport across planetary vorticity contours, $\beta\partial\psi/\partial x$, and the bottom pressure torque, $J(P_b, H)$, in (1); the curl of the boundary stresses is at least an order of magnitude smaller.

In each model, the different spreading of dense water is associated with a different bottom pressure torque and depth-integrated transport. In MOMA, the dense water spreads away from the overflow, at a depth between 1000 m and the bottom, and remains attached to the northwest boundary in the Ionian; see Fig. 11b, and the density and velocity section along 36°N in Fig. 12a. This spreading pattern is associated with a dipole in the bottom pressure torque: negative values in the western Ionian (36°N, 16°E) and positive values in the northern Ionian (39°N,18°E) as shown by the shading in Fig. 12b. These different bottom pressure torques correspond to southern and northern transport respectively, see the streamlines in Fig. 12b.

In contrast, in MICOM, the dense water spreads over the deep channels of the central Ionian, as revealed in Figs. 11b and 12a. This mid-basin spreading of dense water is associated with a bottom pressure torque which is positive in the western Ionian (36°N,16°E) and negative in the central Ionian (35°N,18°E) (Fig. 12b). Consequently, in the western Ionian, both the bottom pressure torque and depth-integrated transport have opposite signs in the MOMA and MICOM integrations.

Hence, the spreading of the dense water appears to be a highly sensitive process: a change in the spreading pattern of dense water is concomitant with a different bottom pressure torque and depth-integrated circulation. In turn, these different depth-integrated circulations lead to contrasting CFC-12 distributions; for example, in MOMA, the recirculating, cyclonic gyre transports high CFC-12 from the western slope into the interior, which leads to anomalously high concentrations between 1000 and 2500 m north of 36°N (Fig. 6b).

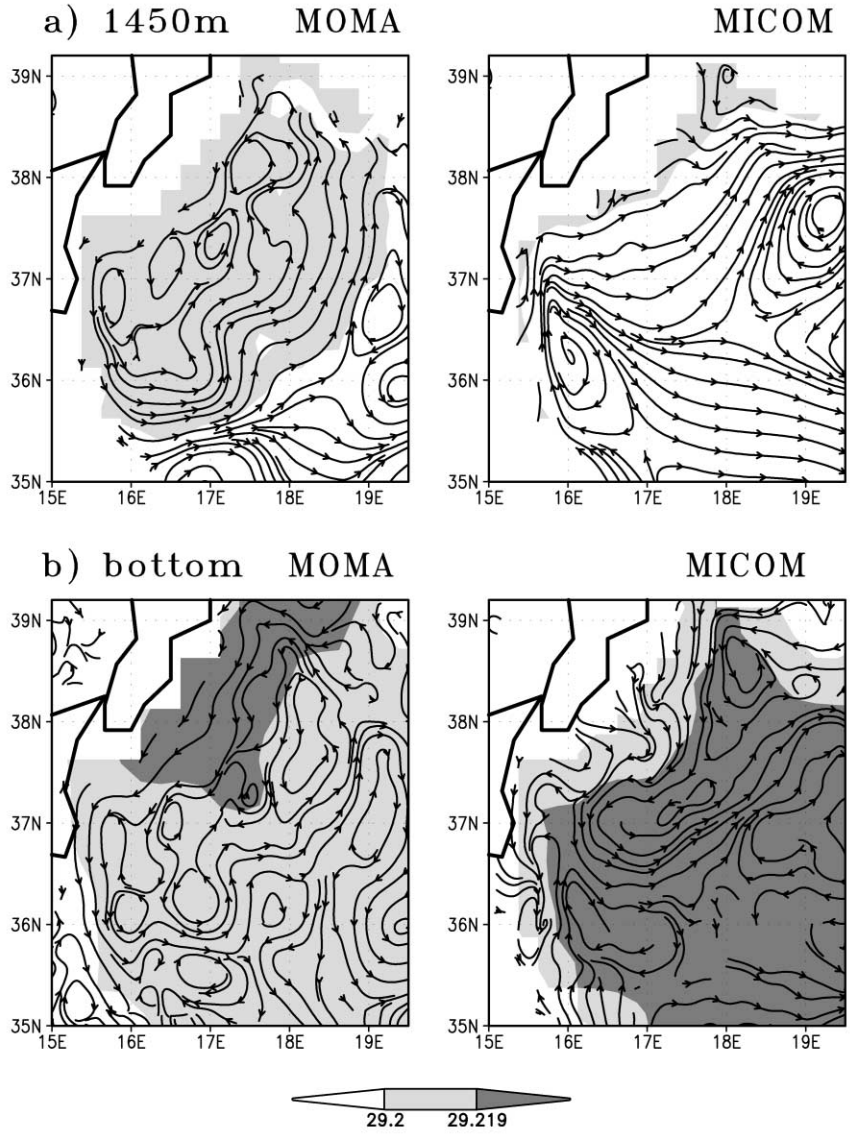

Fig. 11. Streamlines of the velocity (a) 1450 m and (b) sea floor for MOMA and MICOM together with shading showing the potential density. Note in (b) how the dense water spreads along the northwest boundary in MOMA and over the centre of the basin in MICOM.

6. Discussion and conclusion

The thermohaline circulation involves several distinct phases: localized formation of dense water, spreading of dense water through overflows, boundary currents and interior recirculations, and the eventual lightening and return of the dense water. Modelling the thermohaline circulation

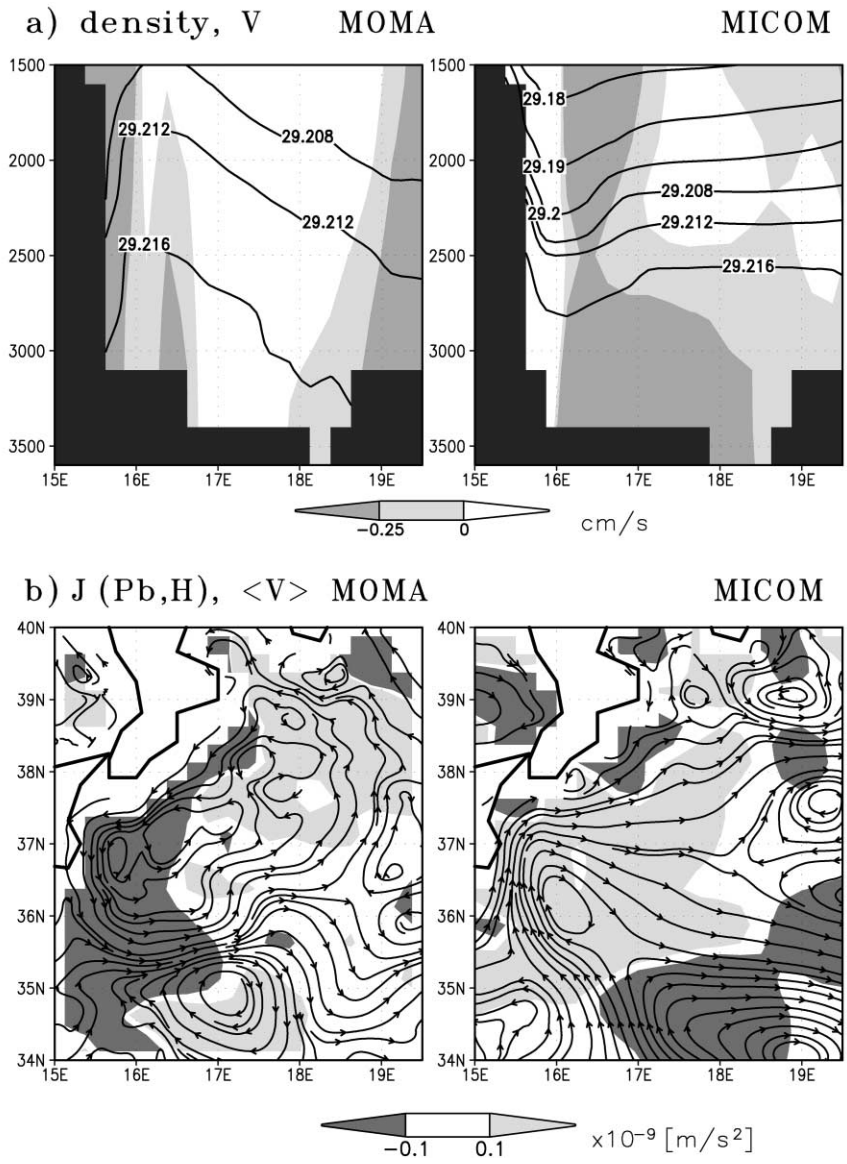

Fig. 12. (a) Zonal section along 36.4°N for density in MOMA and MICOM with shading showing a southwards velocity; (b) streamlines of depth-integrated transport (contours) with shading showing maxima in the bottom pressure torque, $J(P_b, H)$ (light is positive, dark is negative). In MOMA (left panel), dense water spreads away from the overflow along the northwest Ionian, and is associated with $J(P_b, H) < 0$ and southwards transport. In MICOM (right panel), dense water spreads into the central Ionian, with $J(P_b, H) > 0$ and northwards transport along the western Ionian.

is a challenging task due to the wide range of space and time scales involved in the process, and the important role of topography in steering the dense water pathways and controlling mixing.

In this study, we examine the spreading of dense water from the Adriatic using cartesian (MOMA) and isopycnic (MICOM) models, and compare with independent transient-tracer

(CFC-12) observations in 1987. The model results differ according to the model formulation, even though both models are integrated with the same topography, equivalent resolution and similar forcing. The major differences are in how the models represent the overflow of dense water over the stepwise topography and the resulting slope convection process, which leads to a different bottom pressure torque and depth-integrated circulation.

In MOMA, the overflow is represented by a sequence of advective and convective stages. Unrealistic tracer distributions are obtained if the traditional convection scheme is employed involving a vertical homogenization whenever dense water overlies light fluid. Improved results are obtained if a new convection scheme is employed emphasizing how dense water sinks to its neutrally buoyant level (appendix). While adopting this convection scheme does reduce part of the spurious mixing, dense waters still become over-diluted when overflowing topography. In contrast, in MICOM, the dense overflow is naturally represented by dense water propagating down the topography. The fluid does not become hydrodynamically unstable, so no additional mixing occurs.

Observations reveal the importance of mixing and dilution at overflows, which for a number of dense water sources can paradoxically lead to the most dense source water eventually settling out at mid-depths (Price and Baringer, 1994). For our particular case study, the isopycnic model provides a more realistic simulation for the observed transient tracer distribution, than a cartesian model. In the isopycnic model, an improved representation of the overflow process might be obtained by including additional explicit mixing. In contrast, in the cartesian model, the overly high mixing is only likely to be reduced with either a much finer resolution[3] (Winton et al., 1998) or through incorporating an improved bottom boundary layer, such as that developed by Beckmann and Döscher (1997) and applied by Dengg et al. (1999) in the North Atlantic.

Misleading results for the thermohaline circulation can be obtained through a poor representation of overflows. In our study, there is a different spreading of dense water in the cartesian and isopycnic models despite the same wind forcing and topography being applied. The different spreading patterns are concomitant with different signs in the bottom pressure torque and depth-integrated circulation. Consequently, the different model representations lead to far field consequences evident in the model simulations having different transient-tracers distributions throughout the water column.

Acknowledgements

This study was supported by EU grant MAS3-CT96-0051 and supercomputing time from NERC grant GR9/03418. We are grateful for advice from Chris Hughes and pertinent comments from an anonymous reviewer.

[3] Our results support the isopycnic and cartesian model comparison of Winton et al. (1998), who find that there is overly strong mixing in the cartesian model unless the bottom boundary layer and maximum slope of the topography are resolved. This condition requires that the horizontal resolution reaches $\Delta x = \Delta z/\alpha$ where Δz is the vertical resolution and α is the topographic slope. However, for the slope at Otranto, $\alpha \sim 0.03$ and $\Delta z \sim 100$ m, then the horizontal resolution should reach $\Delta x \sim 3$ km, which at present is prohibitive for climate studies.

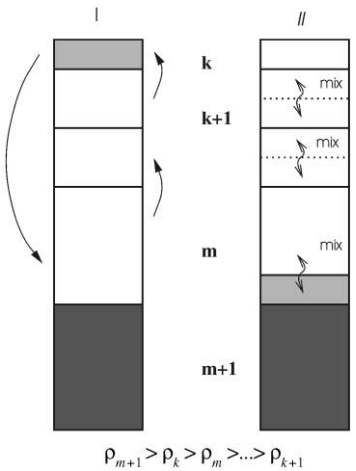

Fig. 13. A schematic of the vertical exchange, convection scheme. When there is static instability with dense fluid at the surface overlying a column of less dense fluid, then (i) dense fluid is transferred from the surface to the level of neutral stability without mixing and the overlying column of lighter fluid is displaced upwards, (ii) the convected dense fluid is mixed with the rest of the box m, and similar volume-weighted mixing occurs within the other overlying boxes.

Appendix. Alternative convection scheme

Convection schemes are required in order to remove static instability and to parameterize the sinking and mixing associated with convection (see review by Marshall and Schott, 1999). The convection scheme is particularly important for cartesian models when dense water overflows topography and slope convection can result.

The most common convection schemes remove static instability by vertical mixing: by increased vertical diffusivity using implicit scheme, or by direct volume-weighted mixing between the neighbouring boxes, or mixing of the overall unstable column. All these parameterizations lead to rapid dilution of the dense waters during slope convection, since the mixing involves horizontal scales much larger than the typical convection scales.

Our alternative convection scheme emphasizes the sinking of dense water and reduces the excessive dilution of dense water when removing static instability (Fig. 13). The scheme is a simplified version of parameterizations developed for atmospheric convection (Arakawa and Schubert, 1974) and oceanic convective plumes (Paluszkiewicz and Romea, 1997).

The modified scheme checks the vertical column for static instability. When dense water overlies lighter water, the dense water is moved to its neutrally buoyant level and the lighter water is displaced upwards throughout the water column (Fig. 13, stage I). The new water column is then partitioned into boxes defined by the fixed model levels. The properties of the different fluid making up each box are simply combined using volume-weighted mixing (Fig. 13, stage II).

The scheme is conservative and removes the static instability. The density anomaly is reduced by the mixing within individual boxes in the scheme, but this dilution is much less than obtained in the standard schemes. Additional entrainment can be included during the sinking, involving plume physics (Turner, 1973), such as in the parameterization developed by Paluszkiewicz and Romea

(1997). However, we choose to avoid adding this entrainment in order to reduce explicit mixing. Note that the convection scheme does not lead to a net transport of volume, but only of properties (i.e. density or tracer concentration). In addition, the amount of property transfer and dilution in the convection scheme is a consequence of the model resolution.

Applying this alternative convection scheme leads to substantial improvement in the transient tracer distribution modelled by MOMA, as revealed by comparing the model simulations in Fig. 4 with the observations in Fig. 2b; the alternative scheme has also been used in a previous CFC-12 simulation of Roether et al. (1994).

References

Arakawa, A., Schubert, W., 1974. Interaction of cumulus cloud ensemble with the large-scale environment. I. Journal of Atmospheric Science 31, 674–701.

Beckmann, A., Döscher, R., 1997. A method for improved representation of dense water spreading over topography in geopotential-coordinate models. Journal of Physical Oceanography 27, 581–591.

Beitzel, V., 1997. Untersuchung der thermohalinen Zirkulation desstlichen Mittelmeeres in einem Bryan-Cox Modell durch Simulation von Freon-12 Verteilungen. Doctoral Dissertation, University of Bremen, Germany, 100pp.

Bleck, R., Smith, L.T., 1990. A wind-driven isopycnic coordinate model of the North and Equatorial Atlantic Ocean. 1. Model development and supporting experiments. Journal of Geophysical Research 95, 3273–3285.

Dengg, J., Böning, C., Ernst, U., Redler, R., Augustin, S., Beckmann, A., 1999. Effects of an improved model representation of overflow water on the subpolar North Atlantic. International WOCE Newsletter 37, 10–15.

DYNAMO, 1997. DYNAMO dynamics of North Atlantic models. DYNAMO Scientific Report No. 3, Grenoble, Southampton and Kiel, 182pp.

Friedrich, H., Levitus, S., 1972. An approximation to the equation of state for sea water suitable for numerical ocean models. Journal of Physical Oceanography 2, 514–517.

Gent, R.P., McWilliams, J.C., 1990. Isopycnal mixing in ocean circulation models. Journal of Physical Oceanography 20, 150–155.

Hughes, C.W., 2000. A theoretical reason to expect inviscid western boundary currents in realistic oceans. Ocean Modelling, in press.

Klein, B., Roether, W., Manca, B., Bregant, D., Beitzel, V., Kovacevic, V., Luchetta, A., 1999. The large deep water transient in the Eastern Mediterranean. Deep-Sea Research I 47, 371–414.

Ledwell, J.R., Watson, A.J., Law, C.S., 1993. Evidence for slow mixing across the pycnocline from an open-ocean tracer-release experiment. Nature 364, 701–703.

Levitus, S., 1982. Climatological Atlas of the World Ocean. NOAA Prof. Paper No. 13, Washington DC, 173pp.

Marshall, J., Schott, F., 1999. Open-ocean convection: observations, theory and models. Reviews of Geophysics 37, 1, 1–64.

Mertz, G., Wright, D.G., 1992. Interpretations of the JEBAR term. Journal of Physical Oceanography 22, 301–305.

Munk, W., Wunsch, C., 1998. Abyssal recipes II: energetics of tidal and wind mixing. Deep-Sea Research I 45, 1977–2010.

Ovchinnkov, I.M., Zats, V.I., Krivosheya, V.G., Udodov, A.I., 1985. Formation of deep Eastern Mediterranean waters in the Adriatic Sea. Oceanology 25, 704–707.

Paluszkiewicz, T., Romea, R.D., 1997. A one-dimensional model for the parameterization of deep convection in the ocean. Dynamics of Atmospheres and Oceans 26, 95–130.

Polzin, K.L., Toole, J.M., Ledwell, J.R., Schmitt, R.W., 1997. Spatial variability of turbulent mixing in the abyssal ocean. Science 276, 93–96.

Price, J.F., Baringer, M.O., 1994. Outflows and deep-water production by marginal seas. Progress in Oceanography 33 (3), 161–200.

Roberts, M.J., Marsh, R., New, A.L., Wood, R.A., 1996. An intercomparison of a Bryan-Cox-type ocean model and an isopycnic ocean model. Part I: the subpolar gyre and high-latitude processes. Journal of Physical Oceanography 26, 1495–1527.

Roether, W.R., Manca, B.B., Klein, B., Bregant, D., Georgopoulos, D., Beitzel, V., Kovacevic, V., Luchetta, A., 1996. Recent changes in Eastern Mediterranean deep waters. Science 271, 333–335.

Roether, W.R., Roussenov, V., Well, R., 1994. A tracer study of the thermohaline circulation of the Eastern Mediterranean. In: Malanotte-Rizzoli, P., Robinson, A.R. (Eds.), Ocean Processes in Climate Dynamics: Global and Mediterranean Examples. Kluwer Academic Publishers, Dordrecht, pp. 371–394.

Roether, W.R., Schlitzer, R., 1991. Eastern Mediterranean deep water renewal on the basis of chlorofluoromethane and tritium data. Dynamics of Atmosphere and Oceans 15, 333–354.

Roussenov, V., Stanev, E., Artale, V., Pinardi, N., 1995. A seasonal model of the Mediterranean Sea general circulation. Journal of Geophysical Research 100, 13515–13538.

Schlitzer, R., Roether, W.R., Oster, H., Junghans, H.G., Hausmann, M., Johannsen, H., Michelato, A., 1991. Chlorofluoromethane and oxygen in the Eastern Mediterranean. Deep-Sea Research 38, 1531–1551.

Stratford, K., 1999. Flux-limited advection for tracers in an Ocean General Circulation Model. Journal of Atmospheric and Oceanic Technology 16, 1284–1298.

Toole, J.M., Schmitt, R.W., Polzin, K.L., Kunze, E., 1997. Near-boundary mixing above the flanks of a midlatitude seamount. Journal of Geophysical Research 102, 947–959.

Turner, J.S., 1973. Buoyancy Effects in Fluids. Cambridge University Press, Cambridge, 367pp.

Warner, M.J., Weiss, R.F., 1985. Solubilities of chlorofluorocarbons 11 and 12 in water and seawater. Deep-Sea Research 32, 1485–1497.

Webb, D.J., Coward, A.C., de Cuevas, B.A., Gwilliam, C.S., 1997. A multiprocessor ocean general circulation model using message passing. Journal of Atmospheric and Oceanic Technology 14, 175–183.

Winton, M., Hallberg, R., Gnanadesikan, A., 1998. Simulation of density-driven frictional downslope flow in z-coordinate ocean models. Journal of Physical Oceanography 28, 2163–2174.

Wu, P., Haines, K., 1996. Modelling the dispersal of Levantine Intermediate Water and its role in Mediterranean deep water formation. Journal of Geophysical Research 101, 6591–6607.

Wüst, G., 1961. On the vertical circulation of the Mediterranean Sea. Journal of Geophysical Research 66, 3261–3271.